Relative dispersion in a model of stratified upper-ocean turbulence

Stefano Berti[1] and Guillaume Lapeyre[2]

[1] Université de Lille, ULR 7512 Unité de Mécanique de Lille - Joseph Boussinesq (UML) - F-59000 Lille, France. Email: stefano.berti@polytech-lille.fr

[2] LMD/IPSL, CNRS/ENS, 24 rue Lhomond, 75005 Paris, France. Email: glapeyre@lmd.ens.fr

Turbulence in the upper ocean in the submesoscale range (scales smaller than the deformation radius) plays an important role for the heat exchange with the atmosphere and for oceanic biogeochemistry. Its dynamical features are thought to strongly depend on the seasonal cycle and the associated mixed-layer instabilities. The latter are particularly relevant in winter and are responsible for the fomation of energetic small scales that are not confined in a thin layer close to the surface, as those arising from mesoscale-driven processes, but extend over the whole depth of the mixed layer. The knowledge of the transport properties of oceanic flows at depth, however, is still limited, due to the complexity of performing measurements below the surface. Relative dispersion can be a useful tool to understand the coupling between the surface and interior dynamics.

Model

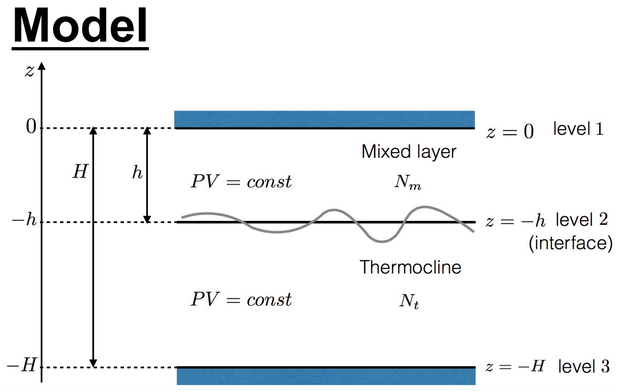

Figure 1: Schematic of the 2 layer model.

We consider a quasi-geostrophic model system (Fig. 1) made of two coupled fluid layers (aimed to represent the mixed layer and the thermocline) with different stratification. Such a model can give rise to both meso and submesoscale instabilities (Fig. 2) and dynamics that compare well with observations of wintertime submesoscale flows [1]. While the former instabilities are due to classical baroclinic instability, the latter are associated with mixed layer instabilities.

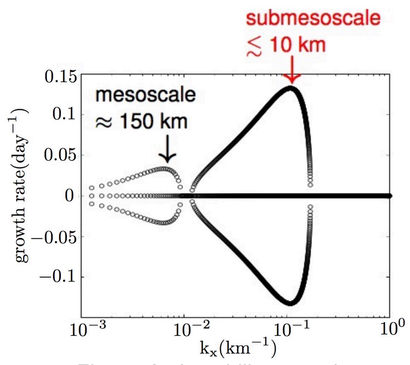

Figure 2: Instability growth rates versus horizontal wavenumber.

The model dynamics are specified by the evolution equation of 3 δ-PV sheets, θ_i (see [1] for more details):

$$\partial_t\theta_i + J(\psi_i,\theta_i) + U_i\partial_x\theta_i + \Gamma_i\partial_x\psi_i = r\nabla^{-2}\theta_i + D_s(\theta_i)$$

mean zonal flows; mean meridional PV gradients; large-scale dissipation; small-scale dissipation

θ_i are related to the buoyancy field by

$$\theta_1 = \frac{-fb(z=0)}{N_m^2};\ \theta_2 = f\left[\frac{b(z=-h^+)}{N_m^2} - \frac{b(z=-h^-)}{N_t^2}\right];\ \theta_3 = \frac{fb(z=-H)}{N_t^2}$$

The QG assumption sets a relation between ψ, b and θ such that $b = f\partial_z\psi$, $\hat{\theta}_i = L_{ij}\hat{\psi}_j$ (with ψ_j the stream-function at depth j), $u = -\partial_y\psi$, $v = \partial_x\psi$. N_m and N_t are the Brunt-Väisälä frequencies of the two layers.

These equations are numerically integrated by means of a pseudospectral method using realistic parameter values, for the (wintertime) midlatitude ocean, on a doubly periodic square domain of side L=500 km at resolution 512^2.

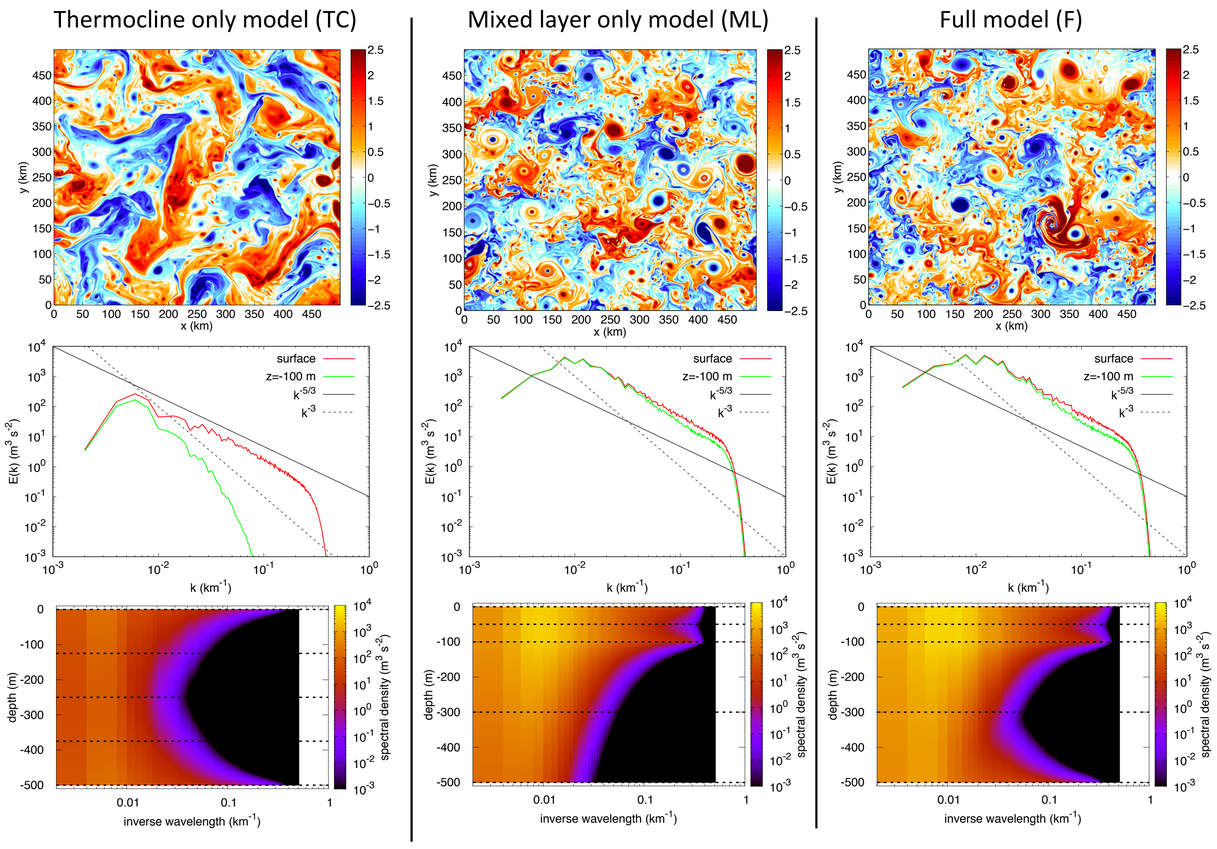

Figure 3: Buoyancy field, normalized by its root-mean-square (rms) value at the surface (z=0) for the three considered cases: TC (h=250 m, H=2h, N_t=N_m), ML (h=100 m, H=10h, N_t=4N_m), F (h=100 m, H=5h, N_t=4N_m). In all cases the vertical shear is Λ_t=Λ_m.

Figure 4: (Top row) Kinetic energy spectra versus horizontal wavenumber at the surface and at depth z=-100 m for the three considered cases. The continuous and dashed lines respectively coorespond to $k^{-5/3}$ and k^{-3} for reference.

(Bottom row) Vertical structure of kinetic energy spectra for the three considered cases. The horizontal dashed lines indicate the depths where the I-kind FSLE (Fig. 5) is computed.

In all the examined cases (TC, ML, F) the turbulent dynamics at the surface are characterized by a broad range of active scales and kinetic energy spectra scaling approximately as $k^{-5/3}$. In the TC case, however, the surface flow has a more filamentary structure and small-scale eddies rapidly decay with depth, with corresponding spectra that are steeper than k^{-3}. In the presence of mixed-layer instabilities (ML, F), the full mixed layer is energized. In the F case, near the bottom, the particularly energetic spectra are due to the SQG-like dynamics at z=-H, as in the TC case.

Lagrangian pair dispersion

In the statistically steady state, the turbulent flows of the different models are seeded with a large number N of Lagrangian tracer particles. At each depth, particles move according to:

$$\dot{\boldsymbol{x}}_i = \boldsymbol{v}\left(\boldsymbol{x}_i(t),t\right);\quad i = 1,...,N$$

$$\boldsymbol{v} = \boldsymbol{u} + \boldsymbol{U} \qquad \boldsymbol{u} = (-\partial_y\psi, \partial_x\psi)$$

where $\boldsymbol{U}$ is the zonal mean flow at the considered depth. These equations are integrated using a 4th order Runge-Kutta scheme and bicubic interpolation of the velocity field at the particle positions. Pair dispersion is analyzed using both fixed-time and fixed-scale indicators. The scaling behaviors from both types of statistics are compatible, however quantitative estimations are more difficult to obtain by analyses based on fixed-time averages, due to the large variability of dispersion in time and with the initial pair location. We then focus on the measurement of the FSLE [2-4], defined as:

$$\lambda(\delta) = \frac{\ln r}{\langle\tau(\delta)\rangle} \qquad \tau(\delta): \delta \longrightarrow r\,\delta$$

The **I-kind** FSLE concerns dispersion of pairs of particles **at the same depth**; the **II-kind** FSLE concerns dispersion of pairs of particles **at different depths**.

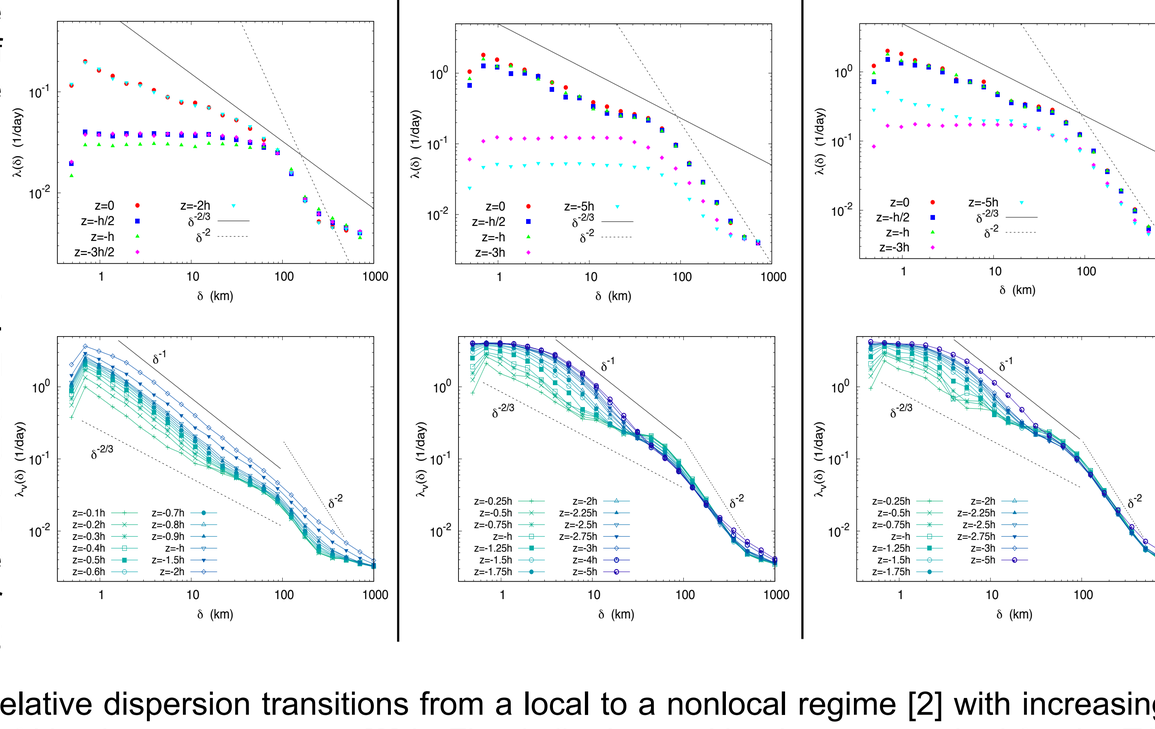

Figure 5: FSLE (I kind) for the three considered cases; here $r = \sqrt{2}$.

For each z, 4096 original pairs are considered. The continuous and dashed lines respectively correspond to $\delta^{-2/3}$ (Richardson local regime) and δ^{-2} (diffusive regime) for reference. Constant FSLE indicates a nonlocal dispersion regime.

Figure 6: FSLE (II kind) for the three considered cases. The settings are as in Fig. 5 but particles in a pair are now selected such that, initially, the first one is at the surface and the second one is at a depth z, with no horizontal separation between them.

We find that relative dispersion transitions from a local to a nonlocal regime [2] with increasing depth, in agreement with the behavior of kinetic energy spectra [3] in Fig. 4. Such transition is more marked for the TC case; in the ML, F cases dispersion is local in the whole mixed layer (Fig. 5). We analyze the correlation between the dispersion properties at the surface and at depth by means of the FSLE-II [4] (Fig. 6). At small depths the FSLE-II behaves similarly to the FSLE-I at separations δ>$O(10)$ km, for the TC case. Due to vertical shear and the less energetic small-scale flow at depth, it gets steeper (scaling ≈ δ^{-1}) at larger depths, first at small separations and then also at larger ones. In the ML and F cases, the FSLE-II is similar to the FSLE-I over a broader range of separations and over the whole mixed layer; at greater depths a steepening, due to vertical shear and smoother deep flow, is observed, as in the TC case. At the largest depths, the FSLE-II tends toward a generic form independent of depth, a point that still needs to be fully understood.

Conclusions

Our preliminary results indicate that, in the absence of a mixed layer, dispersion properties rapidly decorrelate from those at the surface and, due to the missing small-scale flow features and vertical shear, a transition from local to nonlocal dispersion occurs at depth. In the presence of a mixed layer, the dispersion regime is found to be local troughout the mixed layer; below it the less energetic content of small-scale eddies and vertical shear cause a change of behavior at separations <$O(10)$ km. Further developments will be directed to explore in more detail the interplay between 2D turbulence, transport by the mean flow and vertical shear.

References

[1] J. Callies et al., J. Fluid Mech. **788**, 5 (2016).
[2] J. H. LaCasce, Prog. Oceanogr. 77, 1 (2008).
[3] A. Foussard et al., J. Fluid Mech. **821**, 358 (2017).
[4] G. Lacorata et al., Remote Sens. Environ. **221**, 136 (2019).

We are grateful to Sajed Medlej, who contributed to some numerical simulations in the early stage of this study. This work was supported by TOSCA CNES project “New dynamical tools for submesoscales characterization in SWOT data”.